Charge redistribution in core-shell nanoparticles to promote oxygen reduction

Wenjie Tang and Graeme Henkelman[a)]
Department of Chemistry and Biochemistry, The University of Texas at Austin, Austin, Texas 78712-0165, USA

(Received 24 October 2008; accepted 24 April 2009; published online 18 May 2009)

Bimetallic core-shell nanoparticles are a class of near-surface alloy catalyst for which there is a high degree of control over size and composition. A challenge for theory is to understand the relationship between their structure and catalytic function and provide guidelines to design new catalysts that take advantage of material properties arising at the nanoscale. In this work, we use density functional theory to calculate the energetics of oxygen dissociative adsorption on 1 nm Pd-shell nanoparticles with a series of core metals. The barrier for this reaction and the binding energy of atomic oxygen is found to correlate well with the *d*-band level of the surface electrons. Noble metal cores lower the barrier and increase the binding, reducing the activity of the Pd-shell as compared to Pt. Reactive core metals such as Co and Mo, on the other hand, lower the *d*-band of the shell with respect to the Fermi level, giving the Pd-shelled particles oxygen reduction kinetics similar to that of Pt. While both ligand and strain effects determine the *d*-band center of the Pd shell, a greater surface relaxation reduces the strain in nanoparticles as compared to single-crystal near-surface alloys. Charge redistribution between core and shell then becomes an important factor for lowering the *d*-band center of Pd-shelled particles and increasing their activity for the oxygen reduction reaction. © *2009 American Institute of Physics*. [DOI: 10.1063/1.3134684]

I. INTRODUCTION

Fuel cells are attractive power sources because they have the potential to convert chemical to electrical energy with high efficiency. There are, however, several limitations of current proton-exchange membrane fuel cells. The most important issues are related to the catalyst at the cathode. The use of Pt makes fuel cells very expensive, and even the best commercial Pt cathodes have a high overpotential from slow oxygen reduction kinetics, resulting in roughly 30% energy loss.[1] Better and less-expensive catalysts are needed to make the widespread use of low temperature fuel cells viable.

The oxygen reduction reaction (ORR) is a complex reaction involving intermediate states and the transfer of four electrons and protons. Our goal here is not to understand this reaction in detail. Instead, our focus is to understand reactivity trends on model nanoparticle catalysts by looking at a single elementary step—the dissociative adsorption of O_2. This is an important step in the ORR, and we expect that the calculated trends based on this reactivity descriptor will be relevant to more realistic conditions.[2–5] The approach of using reactivity descriptors has been used to successfully characterize new catalysts.[6,7] We should note that the energetics of O_2 dissociative adsorption is not the only possible reactivity descriptor for the ORR or even nessecarily the most important step. Calculations done in the Mavrikakis group indicate that the release of OH is the rate limiting step on Pt and Pt alloys.[8,9] Nevertheless, trends in O and OH binding are similar on transition metal surfaces so that either can be used as a measure of reactivity.[5]

The adsorption of chemical species on metal surfaces can be understood in terms of a model by Hammer and Nørskov.[10] In this model, the interaction between an adsorbate and a metal surface is based on only a few parameters, including the filling, average energy and width of the localized *d*-band of the metal surface, the adsorbate energy levels, and the geometric overlap between the surface and adsorbate orbitals.[3,11] This model is particularly useful for predicting binding energies of an adsorbate in the same binding geometry on different metal surfaces. For this case, the Hammer–Nørskov model predicts a linear relationship between the center of the *d*-band and the binding energy of the adsorbate to the surface.[12] If the *d*-band center is far below the Fermi level, the adsorbate binding is weak. As the *d*-band center approaches the Fermi level, the interaction with the adsorbate increases and it binds more strongly. This model has been verified for oxygen adsorption on a variety of noble and transition metals and alloys.[10,13,14]

Another important trend that holds for catalysts of similar structure is the Brønsted–Evans–Polanyi (BEP) relationship.[15,16] This relationship describes an observation that the energy barrier of an elementary reaction is linearly related to the reaction energy. In the case of oxygen, reactive metals such as Co and Mo bind oxygen very strongly with little or no barrier for dissociative adsorption, whereas noble metals such as Au bind oxygen weakly and have high barriers for dissociative adsorption.[17] When this linear trend between the energy barrier and product binding energy is put into a kinetic model of the surface chemistry, a peak in catalytic activity is found at an optimal compromise between a low reaction barrier and a weak product binding energy.[2,4]

[a)]Electronic mail: henkelman@mail.utexas.edu.

 © 2009 American Institute of Physics

Author complimentary copy. Redistribution subject to AIP license or copyright, see http://jcp.aip.org/jcp/copyright.jsp

Such a peak in activity as a function of reaction energy is called a volcano plot. In the extremes, catalysts with very weak binding have insurmountable barriers and those with strong binding become irreversible covered with reaction product. Effective catalysts provide a balance between these two extremes.

Bimetallic alloys provide a particularly exciting possibility for tuning the reactivity of catalysts. In certain cases, a small amount of one metal can be introduced to a second to form a near-surface alloy (NSA) with catalytic properties that are different and not intermediate to either metal.[6,18] A combination of theoretical and experimental works, particularly in the groups of Mavrikakis and Adzic, have shown that Pt-rich overlays can result in ORR catalysts that are more reactive than Pt.[8,19–21] The general principles governing the reactivity of metal surfaces and applications to catalysis have been reviewed by Groß[22,23] and in a recent comprehensive survey by Nørskov *et al.*[24]

The models that have been established for bulk systems are now being tested at the nanoscale, such as in the recent work on particles with Pt-rich skins by Stamenkovic *et al.*[25,26] and Alayoglu *et al.*[27] The catalytic properties of metal nanoparticles can be very different from bulk metals,[28,29] and the factors which determine the activity of nanoparticles are not well understood.

Here we carry out calculations to determine how the electronic structure of nanoparticles is related to their catalytic activity, and, in particular, if the factors which describe crystal surfaces apply equally to nanoparticles. Tensile strain, for example, is known to play a significant role in determining shifts in the *d*-band of metallic overlayers on crystals,[12,13] but this is not necessarily the case on small nanoparticles where a greater surface relaxation is possible. Core-shell nanoparticles are of particular interest because of their well-defined NSA geometry and because such particles can be synthesized.[30,31]

In this work we compare the energetics of O_2 dissociative adsorption on two model Pd monolayer surfaces: one supported on a slab and the other forming the shell of a 1 nm nanoparticle in the shape of a truncated-octahedral crystallite. Pd was chosen as the catalytic surface because it is electronically similar to Pt, less expensive, and has the potential to be optimized for the ORR through alloying. Pd is less noble than Pt so we have focused on the least-reactive (111) nanoparticle facet. By testing a set of supporting metals, we determine how the ORR energetics and the electronic properties of the Pd surface change and the primary factors which determine the reactivity of the particles.

II. METHODS

Our calculations of oxygen dissociative adsorption on Pd surfaces were done with density functional theory (DFT), using the generalized gradient approximation with the PW91 functional[32] as implemented in the VASP code.[33,34] Valance electrons were treated explicitly in the Kohn–Sham equations[35] and core electrons were described by pseudopotentials with the projector augmented-wave method.[36,37] A plane-wave basis set with an energy cutoff of 274 eV was used for all calculations. Spin polarization was tested in all cases and used as needed, for example, in surfaces containing Co.

Single-crystal surfaces were modeled with four layer slabs containing nine atoms per layer in a $p(3\times3)$ unit cell of the (111) surface. A surface of this size and a vacuum gap of at least 10 Å between slabs were used to sufficiently isolate adsorbed O atoms from their periodic images. A $3\times3\times1$ Monkhost–Pack *k*-point mesh was used to sample the Brillouin zone.[38] The same slab was used to model supported monolayers of Pd on host metal crystals. In two cases a smaller $p(2\times2)$ cell was used: Pd supported on Co (denoted as Co/Pd) to prevent buckling of the highly strained Pd surface and Pd on body centered cubic Mo. This smaller cell was not used for any oxygen adsorption calculations.

Nanoparticles were modeled as a face centered cubic (fcc) crystallite in the shape of a truncated octahedron. The particles were contained in a cubic box of side length 20 Å. Since the particles were isolated by a vacuum gap in all directions, a single Γ-point sampling of the Brillouin zone was used. The 79 atoms in each particle are a magic number for the truncated octahedron shape, which was the lowest energy structure that we found for a pure Pd particle. Core-shell particles were formed by changing the 19 core metal atoms inside the 60-atom Pd shell. For the example of a Pd shell and Co core, the nanoparticle is denoted Co@Pd (using the notation of Ref. 27). For these core-shell particles, the fcc truncated octahedron is not necessarily the lowest energy structure. Our focus here is to consider trends in reactivity due to changes in composition; we have not systematically evaluated the stability of different particle geometries. Such an analysis would be necessary to predict if the nanoparticles could be used as real catalysts.

Stable structures were calculated using force-based energy minimization. The bottom two layers of the slabs were held frozen in their lattice positions, and all atoms in the nanoparticles were relaxed. Geometries were considered optimized when the force on each atom was less than 0.003 eV/Å. Reaction pathways for O_2 dissociative adsorption were found using the climbing-image nudged elastic band method.[39,40]

A Bader analysis was used to quantify the charge around each atom in our calculations.[41,42] Using this analysis, we determined the charge redistribution between the subsurface and the Pd surface and correlated this to the *d*-band center of electrons in the surface.

III. RESULTS

A. Energetics of O_2 dissociative adsorption

The dissociative adsorption mechanism for oxygen on the Pd(111) facet of a Mo@Pd core-shell particle is shown in Fig. 1. The reaction mechanism is similar for each core and slab metal tested. Molecular oxygen binds in the fcc hollow site on a (111) facet aligned in a top-hollow-bridge (t-h-b) geometry. Both oxygen atoms cross bridge sites as the molecule dissociates into adjacent hexagonal close packed (hcp) hollow sites. Energies along the minimum energy path are taken with respect to the gas phase O_2 molecule.

Author complimentary copy. Redistribution subject to AIP license or copyright, see http://jcp.aip.org/jcp/copyright.jsp

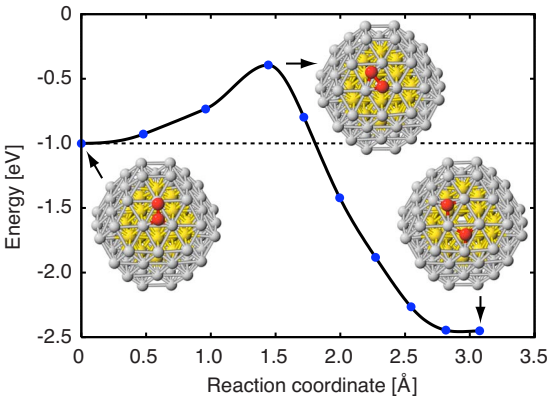

FIG. 1. (Color online) Oxygen dissociation reaction on the (111) facet of the Mo@Pd core-shell particle. Energies are with respect to O_2 in the gas phase. O atoms are red, Pd are gray, and Mo are yellow.

Figure 2 shows the linear correlation between the saddle point energy for O_2 dissociative adsorption and the final state energy with the molecule dissociated on the surface. The Pd-shelled nanoparticles follow the same BEP relationship as single-crystal (111) transition metal surfaces. An ideal catalyst would have both a low barrier and weak product binding (lower right in Fig. 2), but the BEP relationship does not allow this. Instead, there is an optimal trade-off between the dissociation barrier and product binding near Pt(111). Au binds oxygen weakly but the dissociation barrier is prohibitively high. Cu and Pd have low dissociation barriers but bind oxygen too strongly for efficient reduction to water. The same is true for Co and Mo; those points are off the lower-left corner of the plot.

Figure 2 also shows that the core metal inside a Pd shell can be used to tune its interaction with oxygen. The monometallic Pd particle is a little more noble than the Pd(111) surface since it is shifted toward Pt and Au along the BEP relationship. With Au and Ag noble metal cores, the Pd-shell particle becomes less noble, binding oxygen more strongly than the monometallic Pd particle. It is the reactive metal cores, Cu and particularly Mo and Co, which make the Pd shell more noble, closer to Pt(111) on the BEP relationships. These particles are expected to have high ORR catalytic activities.

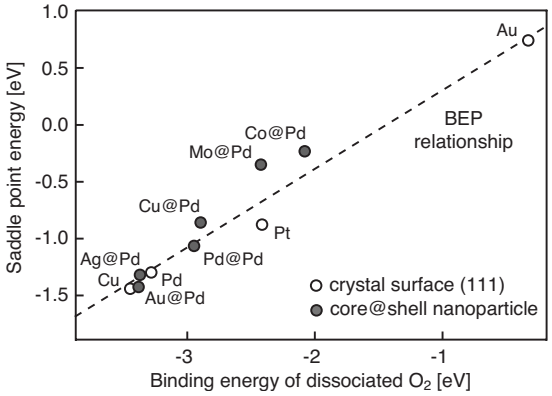

FIG. 2. The saddle point energy for oxygen dissociation on Pd-shelled particles and single-crystal surfaces plotted as a function of the dissociated binding energy of the molecule. The linear trend is a BEP relationship. Particles with barriers and binding energies near Pt(111) are promising catalysts for the ORR.

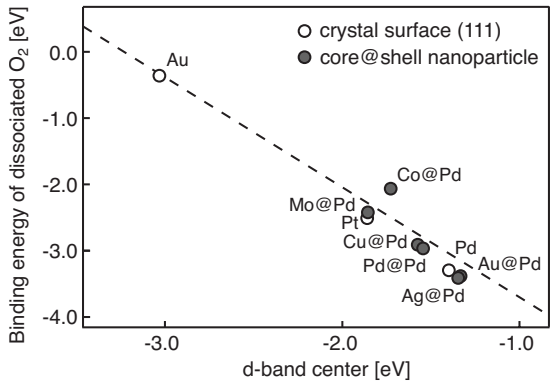

FIG. 3. The binding energy of the dissociated O_2 molecule is linearly related to the average *d*-band energy of electrons in the Pd shell. The same relationship holds for core-shell particles and single-crystal surfaces.

B. Stability of the core-shell nanoparticles

Stability of the core-shell particles is an important issue. There is a serious concern that easily oxidizable cores will dissolve over time in an oxidizing environment. To test particle stability, we exchanged a shell atom with a core atom to see if the binding energy of the particle increased or decreased. Only the Co@Pd particle energy increased, by 0.5 eV, indicating that Co prefers to be in the core. An atom in the Mo core was roughly isoenergetic with the shell; exchange resulted in an energy increase of only 0.15 eV. Moving noble metal atoms (Au and Ag) to the shell decreased the energy by as much as 0.5 eV, showing that these particles are relatively unstable. Fortunately, it is the Co and Mo cores which are the most promising for ORR that are also the most stable. These stability trends are consistent with the surface segregation energy calculations of bulk overlayers by Ruban *et al.*[43]

Another concern is that the adsorption of O (or OH) on the surface could induce core metal atoms into the shell. This is not a problem for Au and Ag which bind O more weakly than Pd. O binds strongly to Co and Mo, however, so that bringing one of these metal atoms from the core to the surface next to an adsorbed O atom is energetically favorable by 0.18 and 1.4 eV, respectively. The Mo@Pd and Co@Pd particles are not thermodynamically stable in an oxidizing environment, but they may be kinetically stable on an experimental time scale at low temperature.

C. Correlation of reactivity with the surface *d*-band

The average *d*-band energy level of the Pd-shell of the core-shell nanoparticles is plotted against the binding energy of dissociated O_2 in Fig. 3. As expected, a lower *d*-band reduces oxygen binding. Furthermore, since the bonding geometries and the surface metal are the same for different core metals, the trend is linear. The same trend is found for single-crystal surfaces showing that oxygen binding is similar between metals and that the *d*-band level is a good single indicator of the surface reactivity. This is consistent with many other calculations.[3,10–13]

Author complimentary copy. Redistribution subject to AIP license or copyright, see http://jcp.aip.org/jcp/copyright.jsp

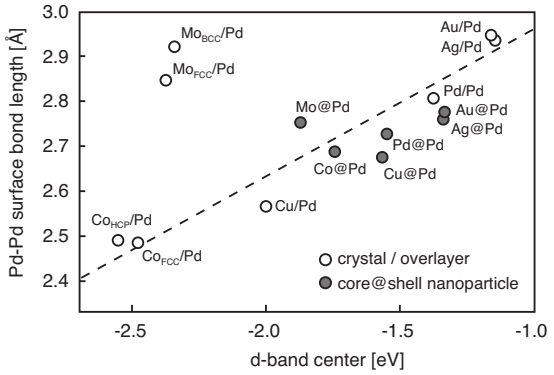

FIG. 4. Plot of the average surface bond length between Pd atoms on the surface of particles and slabs and the center of the surface *d*-band.

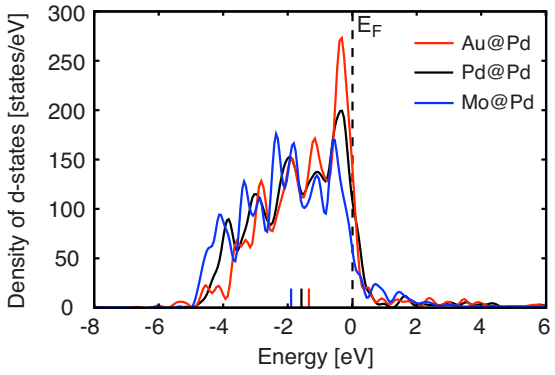

FIG. 5. (Color online) DOS of the Pd surface *d*-band with three core metals. The small vertical marks above the *x*-axis indicate the center of the *d*-bands. The Au core raises the *d*-band level of the Pd shell and Mo lowers it.

D. Strain and ligand effects

The linear trend between the surface *d*-band level and oxygen binding is expected, but it does not provide an explanation for why different core metals shift the *d*-band level of the shell. Two types of effects are used to describe the properties of NSAs, those involving strain in the surface layer,[13] and those involving modifications to the electronic structure of the surface—the so-called ligand effect.[44] An excellent discussion of the distinction between these effects on single-crystal metal surfaces is provided by Kitchin *et al.*[45,46] Strain in the surface layer modifies the reactivity of the surface by changing the width of the *d*-band. A compression of the metal leads to a greater overlap between electrons and a widening of the band, whereas expansion reduces the *d*-orbital overlap and the *d*-band narrows. In order to maintain a constant filling, a widening of band shifts its mean away from the Fermi level, and a narrowing brings the *d*-band center closer. The width of the *d*-band and the *d*-band center is also changed by bonding interactions with alloy metals, which is the ligand effect.

To determine if the strain or ligand effect is causing the change in binding energy in our core-shell particles, we have looked for a correlation between these factors and the *d*-band center. Figure 4 is a plot of the strain in the Pd surface as a function of the *d*-band center. Strain is measured as the average bond length between Pd surface atoms. With the exception of Pd supported on Mo, there is a correlation between the compression of a Pd monolayer on crystals and the lowering of the *d*-band center. For the core-shell nanoparticles, the Pd shell is able to relax to an interatomic spacing that is much closer to bulk Pd (filled circles in Fig. 4). This is expected both because the crystal facets are not constrained laterally, and also because there are 60 Pd shell atoms and only 19 core atoms. Since the Pd–Pd distances in the shell deviate by only a few percent of the monometallic Pd particle, the correlation between strain and the *d*-band center is essentially lost.

Mo and Co are most stable as body centered cubic (bcc) and hexagonal close packed (hcp) structures, respectively. In all calculations, we imposed a fcc lattice for both the slab subsurface and nanoparticle cores. To see if this was biasing our calculations, we did slab calculations in the bcc and hcp structures for Mo and Co, respectively. Figure 4 shows that our results are insensitive to the crystal structure and that the fcc structure does not explain why Mo deviates from the linear trend between strain and the *d*-band level.

Figure 5 shows the *d*-band density of states (DOS) of three Pd-shelled particles. The pure Pd@Pd particle is shown for reference; the Au@Pd particle has the highest *d*-band center and Mo@Pd has the lowest. By inspection, one can see that the width of the *d*-band increases as the *d*-band lowers. It also appears that the DOS of Mo@Pd is shifted to lower energy as compared to Au@Pd, so we tested the constant filling model by quantifying how much the *d*-band center is lowered due to band broadening and band filling from charge redistribution.

Figure 6 shows the linear correlation between the rms *d*-band width and the *d*-band center. To check that the rms width matched the apparent width, we also measured the points at which the DOS crossed a low value of 20 states/eV. This DOS value was chosen to be where the distributions have high slopes so that the widths are well defined. To compare these calculations, we scaled the apparent widths by 27% so that the rms widths most closely matched the apparent widths of the *d*-band. In a rectangular model of the *d*-band, following Ref. 46, the correlation between the rms *d*-band width w and center ϵ_d is a simple function of the *d*-band filling f_d,

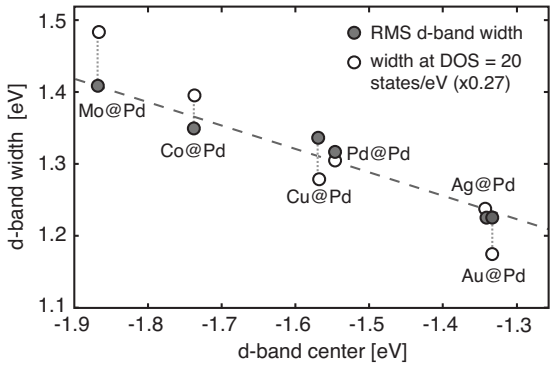

FIG. 6. Correlation between the *d*-band center and width. The *d*-band width was measured in two ways: as the rms width and as a multiple of the DOS value of 20 states/eV.

Author complimentary copy. Redistribution subject to AIP license or copyright, see http://jcp.aip.org/jcp/copyright.jsp

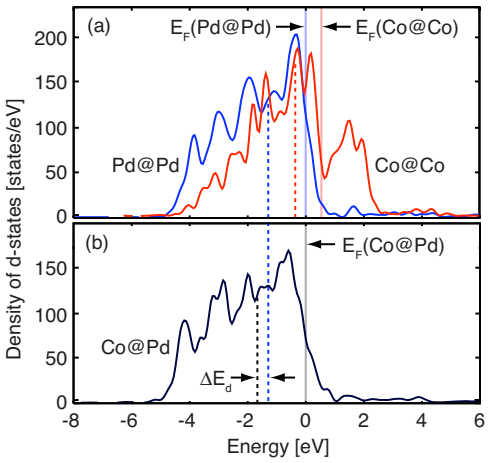

FIG. 7. (Color online) (a) The *d*-band DOS of the shells in monometallic Pd and Co particles. The vertical dashed and solid lines indicate the *d*-band center and Fermi level, respectively. (b) When the Co core and Pd shell are combined, the Fermi level of Co aligns with that of Pd through charge transfer and the *d*-band center of the Pd shell is lowered by ΔE_d.

$$w = \sqrt{\frac{1}{12}}\left(\frac{1}{0.5 - f_d}\right)\epsilon_d. \quad (1)$$

Substituting an average filling of f_d=0.91 for our Pd shells gives an expected slope of −0.70. The rms data in Fig. 6 have a slope of −0.32, significantly smaller in magnitude than expected from the rectangular band model, indicating that there is another factor affecting the *d*-band center.

E. Charge redistribution

We also considered charge redistribution as a factor contributing to the shift in the *d*-band of the Pd shell. By charge redistribution, we mean a shift in charge density between the core metal and the surface rather than the transfer of any single electron in the particle. As two metals with different Fermi levels are brought together, charge will flow from the metal with a higher Fermi level to the lower (or alternatively from the metal with a lower to a higher electronegativity). The Fermi energies of the metals Au, Ag, Pd, Cu, Co, and Mo are calculated by Sigalas *et al.* to be 7.25, 7.48, 7.69, 9.03, 10.52, and 11.36 eV, respectively.[47] The *d*-band levels of the Pd shells follow the same order as the Fermi level of the core metals. Since Au has a lower Fermi energy than Pd, charge is transferred from the Pd shell to the Au core, whereas Cu, Co, and Mo cores donate charge to the Pd surface.

An illustration of how alloying affects the electronic structure of the Pd shell is shown in Fig. 7. In (a) the *d*-band DOSs of Pd and Co shells in monometallic particles are compared. The Fermi level of the Co particle is 0.58 eV above that of the Pd particle. When Co is introduced into the core of the Co@Pd particle (b), the Pd shell accepts electrons from the Co core, lowering the *d*-band of the shell with respect to the Fermi level so that it is uniform throughout the particle.

The possibility of charge transfer has been considered for NSAs in terms of the *d*-band filling.[10] In the work of Kitchin *et al.* charge transfer was considered negligible, in part because the *d*-band filling was found to be nearly constant, and in part because it is difficult to measure the charge of an atom accurately in a unique way.[45,46] These authors calculated the local DOS projected onto a sphere around the atom, and then integrated the fraction below the Fermi level. We have also done this, choosing a sphere with a volume equal to the volume per atom in bulk Pd. The problem with this approach is that the integrated charge is sensitive to the integration radius, and it is not clear how to choose an optimal or consistent value for nanoparticles and alloys. To avoid this ambiguity, we have also used a Bader analysis,[41] employing a grid-based method that is well suited to plane-wave based DFT calculations.[42,48] The strength of the Bader partitioning is that charge is uniquely divided into volumes based on the charge density; there are no free parameters or dependencies on the representation of the wave functions. Figure 8 shows that the Bader charges are consistent with the *d*-band filling calculation in that there is a correlation between the charge transferred to the shell and the lowering of the *d*-band center for core-shell particles. This trend is also present for Pd monolayers although with a greater scatter, perhaps because strain is more important for crystal surfaces.

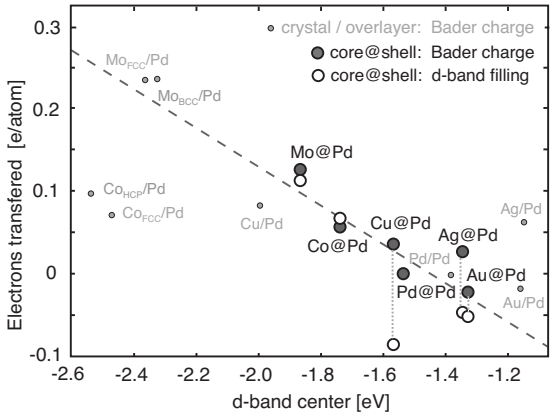

FIG. 8. The amount of charge transferred to the Pd shell is determined by the change in *d*-band filling (open large circles) and the total valance charge within Bader volumes around the Pd atoms (filled large circles). The trend for the core-shell particles, and to a lesser extent Pd monolayers on crystal surfaces (filled small circles), is that as the Pd surface accepts charge from the subsurface metal, the *d*-band center of the surface is lowered.

IV. DICUSSION AND CONCLUSIONS

We have found that both the *d*-band width and filling correlate with the position of the center of the *d*-band and that the *d*-band center can in turn be used as a reactivity indicator for the oxygen dissociation reaction. We can then ask which factor, the width or filling of the *d*-band, is more important for shifting the *d*-band center of the core-shell particles. To address this question, we can decompose the overall shift of 0.5 eV in the *d*-band center of the Pd shell between the particle with the highest value, Au@Pd, and the lowest, Mo@Pd. The widening of the *d*-band is known to be caused by strain. The increase in the rms *d*-band width in the Pd shell between Au@Pd and Mo@Pd is 0.17 eV, which should lower the *d*-band center by 0.24 eV using the rectangular *d*-band model of Eq. (1). This is only half of the observed 0.5 eV shift.

Author complimentary copy. Redistribution subject to AIP license or copyright, see http://jcp.aip.org/jcp/copyright.jsp

The lowering of the *d*-band center due to band filling can be estimated from the amount of charge transfer and the density of *d*-states at the Fermi level. The average difference in charge in the Pd shell atoms between Au@Pd and Mo@Pd is 0.15 e/atom. Figure 5 shows that the DOS at the Fermi level is between 50 and 100 states/eV; the average is 75 or 1.25 states/eV/atom for each of the 60 atoms in the shell. Using this value, charge transfer reduces the *d*-band center in the Pd shell by 0.12 eV. So while the *d*-band width is an important factor for determining the *d*-band level of overlayers on crystals, it is less important for core-shell nanoparticles where strain in the shell is relaxed. For these particles charge redistribution is also important and provides an alternative view of how to tune nanoparticle reactivity. In the case of Pd-shelled particles, cores such as Co and Mo which transfer charge to the shell are good candidates for ORR catalysts.

ACKNOWLEDGMENTS

This work was supported in part by the Robert A. Welch Foundation under Grant No. F-160, the Texas Advanced Research Program, a NSF CAREER Award No. CHE-0645497, and the Texas Advanced Computing Center at the University of Texas at Austin.

[1] T. R. Ralph and M. P. Hogarth, Platin. Met. Rev. **46**, 1 (2001).
[2] J. K. Nørskov, T. Bligaard, A. Logadottir, S. Bahn, L. B. Hansen, M. Bollinger, H. Bengaard, B. Hammer, Z. Sljivancanin, M. Mavrikakis, Y. Xu, S. Dahl, and C. J. H. Jacobsen, J. Catal. **209**, 275 (2002).
[3] J. Greeley, J. K. Nørskov, and M. Mavrikakis, Annu. Rev. Phys. Chem. **53**, 319 (2002).
[4] T. Bligaard, J. K. Nørskov, S. Dahl, J. Matthiesen, C. H. Christensen, and J. Sehested, J. Catal. **224**, 206 (2004).
[5] J. K. Nørskov, J. Rossmeisl, A. Logadottir, L. Lindqvist, J. R. Kitchin, T. Bligaard, and H. Jónsson, J. Phys. Chem. B **108**, 17886 (2004).
[6] J. Greeley and M. Mavrikakis, Nature Mater. **3**, 810 (2004).
[7] A. Nilsson, L. G. M. Pettersson, B. Hammer, T. Bligaard, C. H. Christensen, and J. K. Nørskov, Catal. Lett. **100**, 111 (2005).
[8] J. Zhang, M. B. Vukmirovic, K. Sasaki, A. U. Nilekar, M. Mavrikakis, and R. R. Adzic, J. Am. Chem. Soc. **127**, 12480 (2005).
[9] A. U. Nilekar, Y. Xu, J. Zhang, M. B. Vukmirovic, K. Sasaki, R. R. Adzic, and M. Mavrikakis, Top. Catal. **46**, 276 (2007).
[10] B. Hammer and J. K. Nørskov, Adv. Catal. **45**, 71 (2000).
[11] B. Hammer, L. B. Hansen, and J. K. Nørskov, Phys. Rev. B **59**, 7413 (1999).
[12] A. Ruban, B. Hammer, P. Stoltze, H. L. Skriver, and J. K. Nørskov, J. Mol. Catal. A: Chem. **115**, 421 (1997).
[13] M. Mavrikakis, B. Hammer, and J. K. Nørskov, Phys. Rev. Lett. **81**, 2819 (1998).
[14] Y. Xu, A. V. Ruban, and M. Mavrikakis, J. Am. Chem. Soc. **126**, 4717 (2004).
[15] J. N. Brönsted, Chem. Rev. (Washington, D.C.) **5**, 231 (1928).
[16] M. G. Evans and N. P. Polanyi, Trans. Faraday Soc. **34**, 11 (1938).
[17] B. Hammer and J. K. Nørskov, *Chemisorption and Reactivity on Supported Clusters and Thin Films* (Kluwer, Amsterdam, 1976), pp. 285–351.
[18] F. Besenbacher, I. Chorkendorff, B. S. Clausen, B. Hammer, A. M. Molenbroek, J. K. Nørskov, and I. Stensgaard, Science **279**, 1913 (1998).
[19] J. Zhang, M. B. Vukmirovic, Y. Xu, M. Mavrikakis, and R. R. Adzic, Angew. Chem. **44**, 2132 (2005).
[20] R. R. Adzic, J. Zhang, K. Sasaki, M. B. Vukmirovic, M. Shao, J. X. Wang, A. U. Nilekar, M. Mavrikakis, J. A. Valerio, and F. Uribe, Top. Catal. **46**, 249 (2007).
[21] A. U. Nilekar and M. Mavrikakis, Surf. Sci. **602**, L89 (2008).
[22] A. Groß, Top. Catal. **37**, 29 (2006).
[23] A. Groß, J. Phys.: Condens. Matter **21**, 084205 (2009).
[24] J. K. Nørskov, T. Bligaard, J. Rossmeisl, and C. H. Christensen, Nat. Chem. **1**, 37 (2009).
[25] V. R. Stamenkovic, B. S. Mun, M. Arenz, K. J. J. Mayrhofers, C. A. Lucas, G. Wang, P. N. Ross, and N. M. Marković, Nature Mater. **6**, 241 (2007).
[26] V. R. Stamenkovic, B. Fowler, B. S. Mun, G. Wang, P. N. Ross, C. A. Lucas, and N. M. Marković, Science **315**, 493 (2007).
[27] S. Alayoglu, A. U. Nilekar, M. Mavrikakis, and B. Eichhorn, Nature Mater. **7**, 333 (2008).
[28] A. Ueda and M. Haruta, Gold Bull. **32**, 3 (1999).
[29] M. Valden, X. Lai, and D. W. Goodman, Science **281**, 1647 (1998).
[30] R. W. J. Scott, O. M. Wilson, S.-K. Oh, E. A. Kenik, and R. M. Crooks, J. Am. Chem. Soc. **126**, 15583 (2004).
[31] O. M. Wilson, R. W. J. Scott, J. C. Garcia-Martinez, and R. M. Crooks, J. Am. Chem. Soc. **127**, 1015 (2005).
[32] J. P. Perdew and Y. Wang, Phys. Rev. B **45**, 13244 (1992).
[33] G. Kresse, Phys. Rev. B **62**, 8295 (2000).
[34] G. Kresse and J. Hafner, Surf. Sci. **459**, 287 (2000).
[35] G. Kresse and J. Furthmüller, Comput. Mater. Sci. **6**, 15 (1996).
[36] P. E. Blöchl, Phys. Rev. B **50**, 17953 (1994).
[37] G. Kresse and J. Joubert, Phys. Rev. B **59**, 1758 (1999).
[38] H. J. Monkhorst and J. D. Pack, Phys. Rev. B **13**, 5188 (1976).
[39] G. Henkelman, B. P. Uberuaga, and H. Jónsson, J. Chem. Phys. **113**, 9901 (2000).
[40] G. Henkelman and H. Jónsson, J. Chem. Phys. **113**, 9978 (2000).
[41] R. F. W. Bader, *Atoms in Molecules: A Quantum Theory* (Oxford University Press, New York, 1990).
[42] W. Tang, E. Sanville, and G. Henkelman, J. Phys.: Condens. Matter **21**, 084204 (2009).
[43] A. V. Ruban, H. L. Skriver, and J. K. Nørskov, Phys. Rev. B **59**, 15990 (1999).
[44] B. Hammer and J. K. Nørskov, Surf. Sci. **343**, 211 (1995).
[45] J. Kitchin, J. K. Nørskov, M. A. Barteau, and J. G. Chen, Phys. Rev. Lett. **93**, 156801 (2004).
[46] J. Kitchin, J. K. Nørskov, M. A. Barteau, and J. G. Chen, J. Chem. Phys. **120**, 10240 (2004).
[47] M. Sigalas, D. A. Papaconstantopoulos, and N. C. Bacalis, Phys. Rev. B **45**, 5777 (1992).
[48] G. Henkelman, A. Arnaldsson, and H. Jónsson, Comput. Mater. Sci. **36**, 354 (2006).

Author complimentary copy. Redistribution subject to AIP license or copyright, see http://jcp.aip.org/jcp/copyright.jsp